Turkish Journal of Chemistry

http://journals.tubitak.gov.tr/chem/

Research Article

Turk J Chem
(2017) 41: 548 – 558

doi:10.3906/kim-1701-28

Synchrotron X-ray diffraction studies of β-$Ca_{2-x}M_xSiO_4$ (M = Mg and Sr)

Anti PRODJOSANTOSO[1,*], Brendan KENNEDY[2]
[1]Department of Chemistry, Yogyakarta State University, Yogyakarta, Indonesia
[2]Department of Inorganic Chemistry, University of Sydney, Sydney, Australia

Received: 12.01.2017 • **Accepted/Published Online:** 03.03.2017 • **Final Version:** 05.09.2017

Abstract: The structures of Mg- and Sr-doped β-Ca_2SiO_4 have been established from high-resolution synchrotron X-ray powder diffraction. These silicates are all isostructural and the structures have been refined in the monoclinic space group, $P2_1/n$. As expected based on size arguments, the cell parameters increase as the amount of Sr increases and likewise decrease as the amount of Mg increases due the size effects of the dopant cation. In all cases the SiO_4 tetrahedra are essentially regular.

Key words: Portland cement, larnite, cation doping, X-ray diffraction, ceramics

1. Introduction

Dicalcium silicate Ca_2SiO_4 is a component of Portland cement clinker and is under study for use as a host in inorganic phosphors.[1,2] It has been proposed that it may be a suitable host to contain heavy metals from industrial waste.[3] Ca_2SiO_4 has complex crystal chemistry with five phases described in the literature (α, $\alpha\prime_H$, $\alpha\prime_L$, β, and γ phases).[4,5] Two of these phases occur naturally as the minerals larnite (β-Ca_2SiO_4 monoclinic space group $P2_1/n$) and calcio-olivine (γ-Ca_2SiO_4 orthorhombic space group $Pbnm$). Synthetic Ca_2SiO_4 is usually prepared by the solid-state reaction of CaO or $CaCO_3$ and SiO_2 at temperatures over 1450 °C.[6] Cooling from 1450 °C to room temperature typically yields γ-Ca_2SiO_4,[4,7] whereas annealing γ-Ca_2SiO_4 at lower temperatures can induce a transition to β-Ca_2SiO_4, although the conversion is often incomplete.

There have been numerous attempts to prepare phase-pure β-Ca_2SiO_4 but the results are inconsistent. Efforts include dehydration of calcium silicate hydrate at low temperatures (~800 °C),[6,8] or the use of more reactive starting materials such as $Ca(NO_3)_2$ and colloidal silica at 750 °C.[9,10] Although it is generally accepted that β-Ca_2SiO_4 does not form during heating but rather appears as a metastable phase in the stability field of the γ-Ca_2SiO_4 during cooling,[11] it has been reported that reacting CaC_2O_4 with amorphous SiO_2 at 950 °C under a CO_2 atmosphere produces pure β-Ca_2SiO_4 powders.[12] A more promising means of preparing single-phase samples with the orthorhombic β structure is by the addition of dopant cations including Na, K, Fe, Cr, and B. To date, the role of impurity cations in stabilizing β-Ca_2SiO_4 has not been fully established.[13,14]

Natural larnite was first reported by Tilley[15] in 1929 and the structure of β-Ca_2SiO_4 has been of interest since.[7,16–20] The structure consists of a framework of interconnected Ca polyhedra and isolated [SiO_4] tetrahedra.[21] Early studies by Midgley[18] and Cruickshank[16] suggested there was a large distortion in the SiO_4 tetrahedra, a conclusion disproven in more recent studies. Jost et al.[17] studied the structure of β-Ca_2SiO_4

*Correspondence: prodjosantoso@uny.ac.id

using single-crystal X-ray methods and showed that the SiO_4 tetrahedra were, as expected, regular. Mumme et al.[19,20] and Berliner et al.[22] refined the structure of β-Ca_2SiO_4 using synchrotron X-ray and neutron powder diffraction data. In that work, the β-Ca_2SiO_4 structure was stabilized by the addition of 0.5 wt.% of Cr_2O_3 or 0.4 wt.% of B_2O_3.

Orthorhombic and monoclinic forms of Mg_2SiO_4 have also been reported.[23,24] While orthorhombic Mg_2SiO_4 is isostructural with γ-Ca_2SiO_4, the two monoclinic structures are not isostructural with monoclinic β-Mg_2SiO_4 described in space group $C2/m$. It is possible that Mg-doped β-Ca_2SiO_4 is formed during the production of Portland cement. This is expected to be a minor phase since the temperature employed in the manufacturing of the clinker is usually limited to around 1400 °C.

Carlson[25] and Bickle[26] postulated that Sr-doped β- or α'_L-Ca_2SiO_4 may be formed in cement, if Sr is present in the raw materials. The crystal structure of β-Sr_2SiO_4 has been reported and it is closely related to β-Ca_2SiO_4.[27,28] A comprehensive experimental study of the binary β-$Ca_xSr_{2-x}SiO_4$ system does not appear to have been undertaken to date, although the solid solutions with the α'-structure have been investigated.[29] Recent first-principle calculations of Sr doped β-Ca_2SiO_4 have been reported.[30] In this system, the α'-phase of $Ca_xSr_{2-x}SiO_4$ shows two stability fields for $0 \leq x \leq 0.03$ and for $0.90 \leq x \leq 0.96$. Presumably the α'-structure also exists for contents up to $x = 1$. In all cases a small amount of γ-phase is also observed.[9,10]

$\beta-Ca_2SiO_4$ is believed to be a desirable component in many types of cement, and consequently its production has gained considerable attention. One method used to increase the amount of β-Ca_2SiO_4 present in cement has been to add trace amounts of secondary cations.[31] The present work describes the synthesis of a series of Mg- and Sr-doped β-Ca_2SiO_4 oxides prepared at a low temperature (950 °C)[12] using $MgCO_3$ or $SrCO_3$, $CaCO_3$, and SiO_2 as raw materials, and aspects of their crystal chemistry.

2. Results and discussion

2.1. Electron microscopy

Scanning electron micrographs of selected β-$Ca_{2-x}M_xSiO_4$ (M = Mg or Sr) samples (Figures 1a–1c) show that the materials consist of particles of a wide range of sizes without any dominant features. The homogeneity of the samples was checked using the energy dispersive analysis (EDA) technique. These measurements revealed that the bulk compositions of the materials are as expected (Table 1). The small discrepancies in the Sr:Si ratios for the Sr-doped samples are probably due to the overlap of the Sr and Si lines in the EDA.

2.2. X-ray diffraction studies

The powder X-ray diffraction patterns for β-$Ca_{2-x}Mg_xSiO_4$, x = 0, 0.01, 0.025, 0.04, 0.05, 0.1, and 0.25, recorded using the wavelength of the X-ray CuKα = 1.54178 Å on a Bragg–Brentano diffractometer, are shown in Figures 2a–2g, respectively. The patterns indicate the presence of SiO_2, α'_L-Ca_2SiO_4, and MgO at Mg contents greater than 0.05. The *200* Bragg reflection of MgO at $2\theta = 42.92°$ is the most sensitive indication of the solubility limit.

In the case of the Sr-doped samples, there is no evidence for any unreacted Sr or SiO_2 in the $x = 0.1$ sample (Figure 3e); rather, at this level, excess Sr results in the formation of α'_L-$Sr_xCa_{2-x}SiO_4$ as seen by the strongest *260* Bragg reflection at $2\theta = 33.42°$. Since the β-phase is the phase present in Portland cement, we have limited our studies to compositions with $x \leq 0.1$, as that is where the samples contain only the β-phase. In both series increasing amounts of Mg or Sr resulted in shifts in the Bragg reflections, indicating contraction

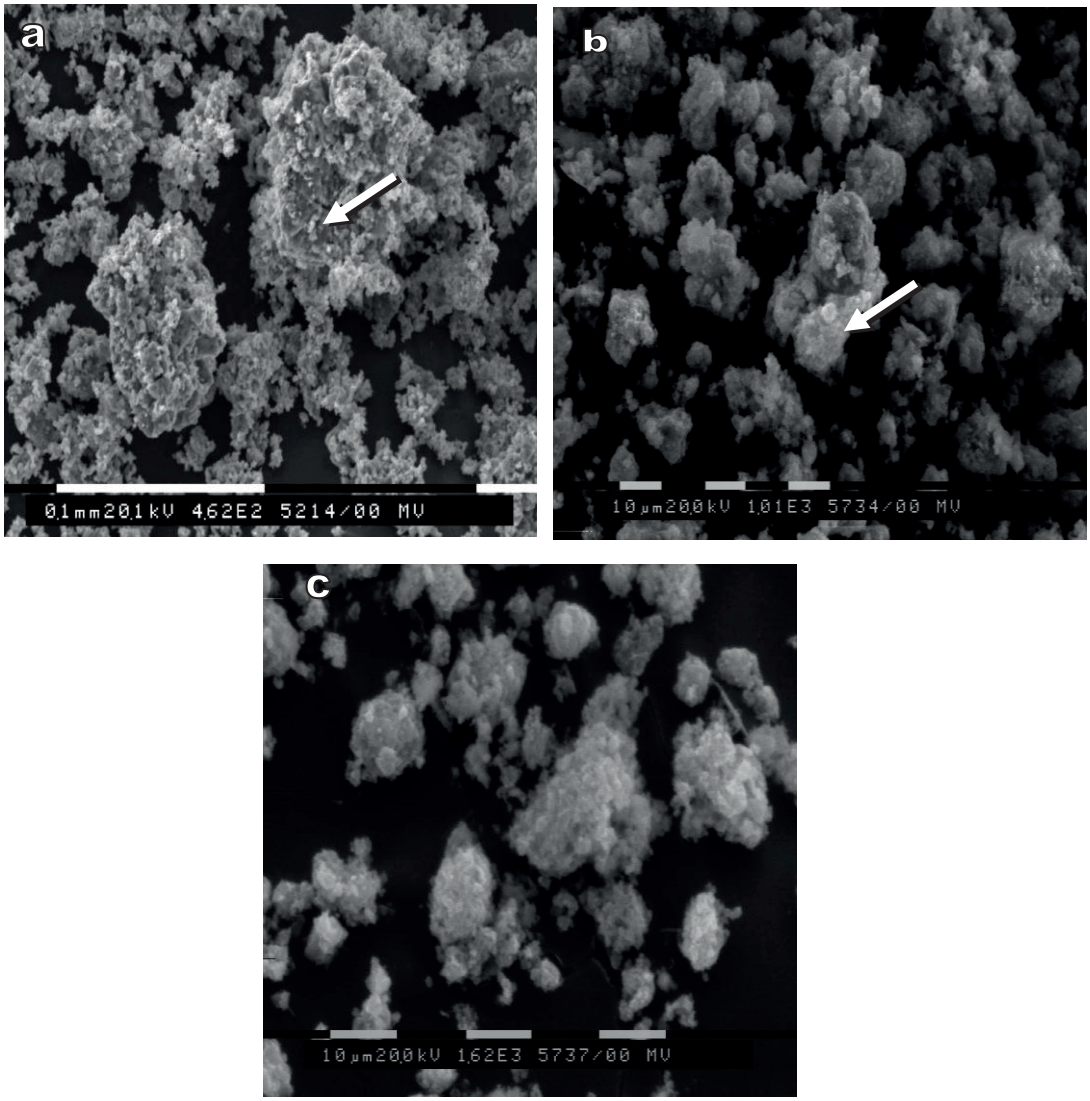

Figure 1. Scanning electron micrographs for (a) β-$Ca_{1.975}Mg_{0.025}SiO_4$, (b) β-Ca_2SiO_4, and (c) β-$Ca_{1.975}Sr_{0.025}SiO_4$. The arrows show the area used for EDA.

Table 1. Observed Ca, Mg, and Si atomic ratios in β-$Ca_{2-x}M_xSiO_4$, M = Mg and Sr, obtained using EDA measurements (e.s.d. ± 0.005).

$Ca_{2-x}M_xSiO_4$, x =	Atomic ratio		
	Ca	M	Si
M = Mg			
0.01	1.97	0.02	1.01
0.025	1.97	0.04	0.99
0.05	1.94	0.05	1.01
0.1	1.92	0.10	0.98
M = Sr			
0	2.03	0	0.97
0.01	1.98	0.05	0.97
0.025	1.96	0.07	0.97
0.05	1.93	0.08	0.99

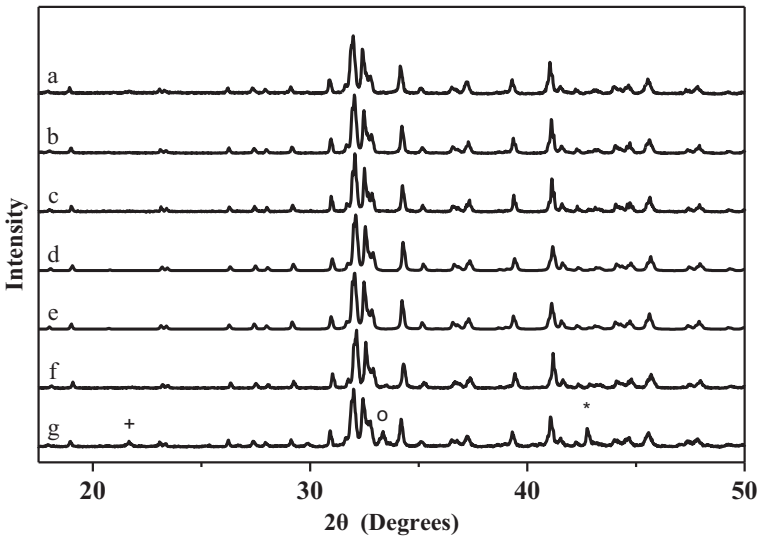

Figure 2. Powder X-ray diffraction patterns of β-$Ca_{2-x}Mg_xSiO_4$ with x = (a) 0, (b) 0.01, (c) 0.025, (d) 0.04, (e) 0.05, (f) 0.1, and (g) 0.25. + indicates the second phase of SiO_2 crystallites, while * indicates MgO and $^{\circ}\alpha'_L$-Ca_2SiO_4.

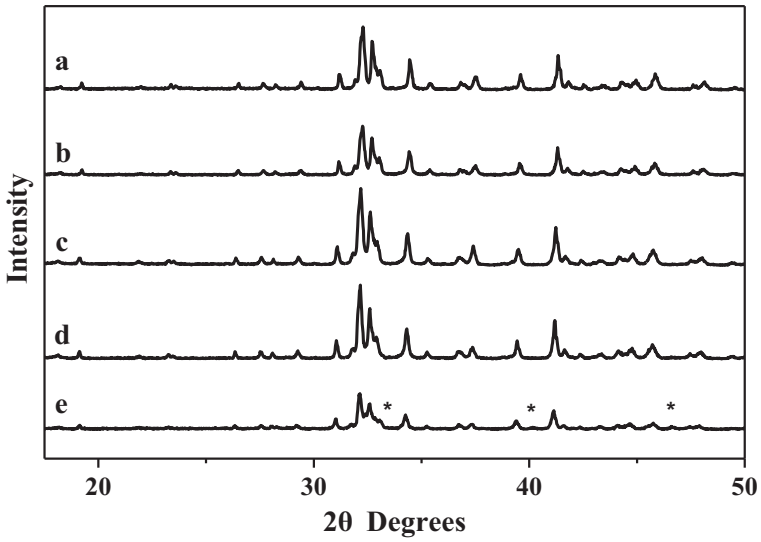

Figure 3. Powder X-ray diffraction patterns of β-$Ca_{2-x}Sr_xSiO_4$, with x = (a) 0, (b) 0.01, (c) 0.025, (d) 0.05, and (e) 0.1. *indicates α'_L-phase of β-$Ca_{2-x}Sr_xSiO_4$.

or expansion of the lattice, respectively, demonstrating that the dopant cation has been incorporated into the lattice.

2.3. Structural refinements

The high-resolution synchrotron X-ray diffraction data for β-$Ca_{2-x}M_xSiO_4$, $x = 0$, 0.01, and 0.025 did not show any evidence of the presence of additional phases. The final refined parameters for all the samples studied are given in Table 2 and representative Rietveld profiles are illustrated in Figures 4a–4c. The Ca cations occupy two crystallographically distinct sites in the monoclinic β-Ca_2SiO_4 structure. The Ca(2) atoms are positioned alternately above and below the SiO_4 tetrahedra in the b direction. The structure may therefore be regarded

as strings of alternating Ca ions and SiO_4 tetrahedra. The strings are linked by the Ca(1) atoms, which are accommodated in the holes between the SiO_4 tetrahedra. The structural refinements demonstrate that the Sr preferentially occupies the 7-coordinate $M(1)$ sites. This is consistent with recent first-principle calculations that concluded doping at the Ca(1) site will be favored.[30]

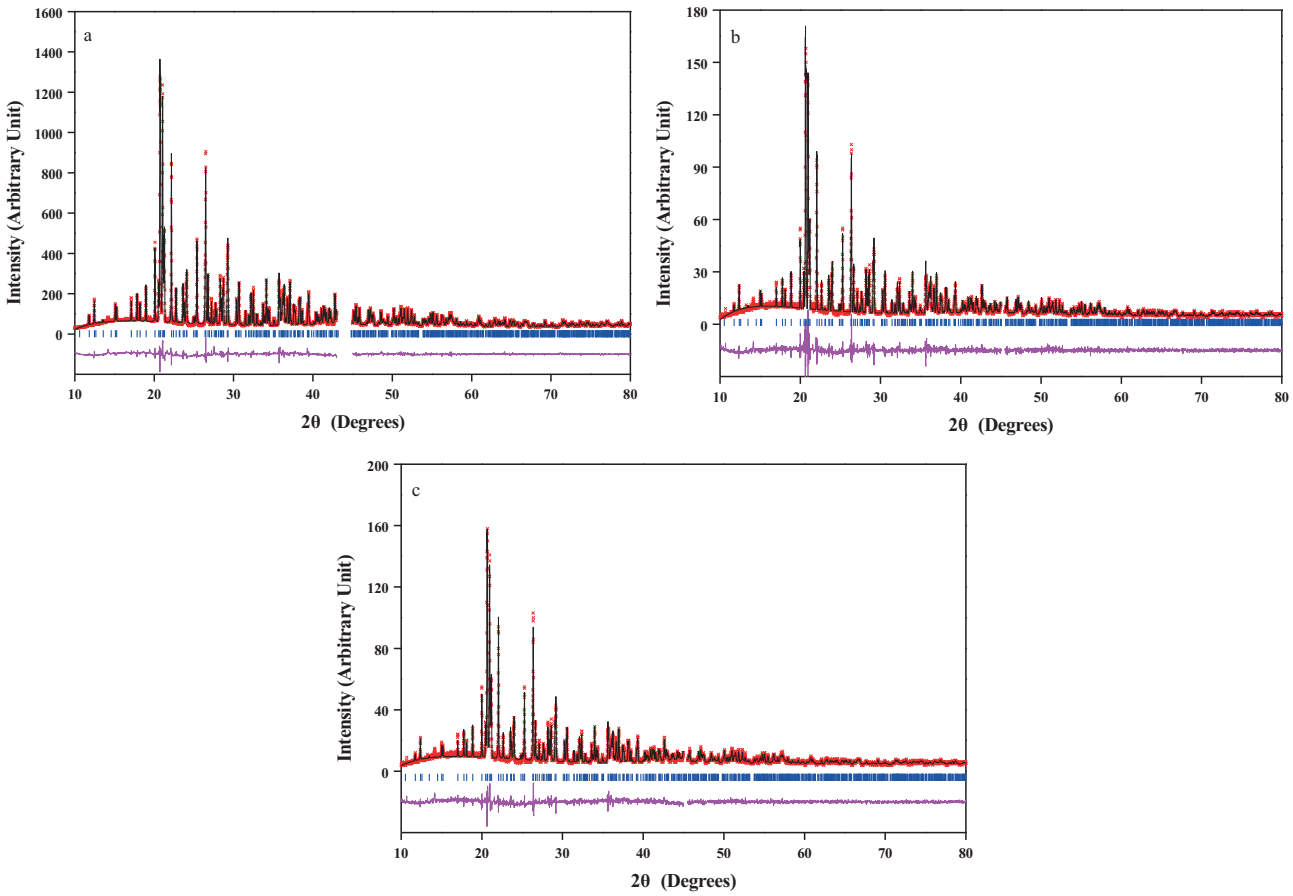

Figure 4. Observed, calculated, and difference synchrotron X-ray diffraction profiles for (a) β-$Ca_{1.975}Mg_{0.025}SiO_4$, (b) β-Ca_2SiO_4, and (c) β-$Ca_{1.975}Sr_{0.025}SiO_4$. The discontinuity in the profile at $\sim 45^\circ$ in each pattern is due to the image plates.

Table 2. Refined structural parameters for β-$Ca_{2-x}M_xSiO_4$, M = Mg and Sr.

	x	a (Å)	b (Å)	c(Å)	β (^{o})	Vol (Å^3)	n$^\#$ values for M		R_p (%)	R_{wp} (%)
							$M(1)$	$M(2)$		
$\beta-Ca_{2-x}Mg_xSiO_4$	0.01	5.5084(1)	6.7552(1)	9.3110(1)	94.489(1)	345.40(1)	0.23(4)	-	4.82	5.62
	0.025	5.5076(1)	6.7539(1)	9.3095(2)	94.505(1)	345.23(1)	0.24(3)	-	4.60	5.54
$\beta-Ca_{2-x}Sr_xSiO_4$	0	5.5053(3)	6.7516(3)	9.3064(4)	94.487(1)	344.86(3)	-	-	7.38	9.17
	0.01	5.5083(2)	6.7569(2)	9.3121(3)	94.450(1)	345.54(2)	-	0.17(9)	7.08	8.84
	0.025	5.5107(1)	6.7621(2)	9.3161(3)	94.421(1)	346.12(2)	-	0.28(8)	7.53	9.41

$^\#$If fully occupied n = 4.

The refined value for occupancy by the Mg of the $4a$ site in $Ca_{1.99}Mg_{0.01}SiO_4$ corresponds to an x value of 0.028. This is higher than the actual stoichiometry and possibly reflects problems in detecting trace amounts of the very light Mg in these compounds. Despite the problems with obtaining an accurate value for the Mg

occupancy, this value implies that all the Mg has occupied the $M(1)$ site. For the Sr-containing compounds, the refined occupancy factors correspond to $x = 0.02 \pm 0.01$ for the $x = 0.01$ sample, which is reasonable. The refined atomic coordinates, selected interatomic distances, and bond angles are given in Tables 3–5, respectively.

Table 3. Refined positional and atomic displacement parameters for β-$Ca_{2-x}M_xSiO_4$.

	$\beta-Ca_{1.975}Mg_{0.025}SiO_4$				$\beta-Ca_{1.99}Mg_{0.01}SiO_4$			
Atoms	x/a	y/b	z/c	B (Å^2)	x/a	y/b	z/c	B (Å^2)
$M(1)$	0.2719(2)	0.3423(1)	0.5693(1)	0.36(3)	0.2719(2)	0.3423(1)	0.5693(1)	0.39(3)
$M(2)$	0.2782(2)	0.9981(2)	0.2982(1)	0.53(3)	0.2784(2)	0.9980(2)	0.2984(1)	0.59(3)
Si	0.2321(3)	0.7818(2)	0.5815(2)	0.45(4)	0.2321(3)	0.7818(2)	0.5815(2)	0.54(5)
O(1)	0.2856(5)	0.0111(4)	0.5575(3)	0.72(7)	0.2844(5)	0.0119(4)	0.5577(3)	0.78(7)
O(2)	0.0187(6)	0.7475(4)	0.6916(3)	0.71(7)	0.0185(6)	0.7484(4)	0.6912(3)	0.89(7)
O(3)	0.4822(6)	0.6691(5)	0.6367(3)	0.97(7)	0.4825(6)	0.6700(5)	0.6370(3)	1.08(7)
O(4)	0.1556(5)	0.6735(5)	0.4277(3)	0.91(7)	0.1556(5)	0.6727(5)	0.4278(3)	0.94(7)

As noted above, the β-$Ca_{2-x}M_xSiO_4$ structure (Figure 5) is built up of isolated SiO_4 tetrahedra and two crystallographically distinct Ca ions. It is considered that all the oxygen atoms within 2.9 Å of a Ca/Sr cation are assumed to belong to its coordination sphere. Oxygen atoms outside this sphere are at distances greater than 3.15 Å from the cation. The coordination of the $M(1)$ cation site is irregular with seven nearest neighbors contributed by four surrounding SiO_4 tetrahedra at distances ranging between 2.236(6) Å and 2.870(6) Å. The second type of cation, M(2), has a SiO_4 tetrahedron positioned immediately above and below it in the b direction, and it is surrounded by three more SiO_4 tetrahedra at approximately the same displacement along b. The coordination of the M(2) site is again irregular, with eight nearest oxygen atoms at distances between 2.375(3) Å and 2.666(6) Å. It is worth mentioning that the mean M(1)–O distances are slightly longer, $\sim$0.02 Å, than that of M(2)–O (Table 4). This is consistent with the lower coordination number of Ca(1).

The values found here for the Si–O distances in undoped β-Ca_2SiO_4 are slightly shorter than those obtained by Jost et al.[17] However, as found by Jost et al., they demonstrate the SiO_4 tetrahedra to be essentially regular with only minimal distortion and this agrees with the observation by Mumme et al.[19,20] that the Si–O distances vary over a small range, between 1.61 and 1.66 Å. In contrast, the refined lattice parameters for β-Ca_2SiO_4 are slightly, but not significantly, larger than those reported by Jost et al.[17] and they are marginally smaller than those reported by Mumme et al.[19,20] (Table 2). The interatomic distances and angles within the SiO_4 tetrahedra in the β-$Ca_{2-x}M_xSiO_4$ series are given in Tables 4 and 5. The Si–O(1) distance is slightly shorter than the other three Si–O distances. This can be explained due to the weaker interactions of O(1) in the $(Ca/M)O_x$ polyhedra. In contrast, the Si–O(4) distances in all series are longer than the other three Si–O distances. The O(1) atoms are coordinated by four nearest neighbors, i.e. Ca(1), Ca(2), Ca(2)′, and Si, with three oxygen atoms, O(2), O(3), and O(4), nearby, while O(4) bonds to one Si and four Ca atoms, Ca(1), Ca(1)′, Ca(2), Ca(2)′, and Si, with three close oxygen contacts to O(1), O(2), and O(3). The distances are shown in Table 4. As expected, the mean Si–O distances are considerably shorter than the mean Ca–O distances due to the smaller size and lower coordination number of the Si. Considering all the compounds then it is unclear if the dopant cation influences the strength of the Si–O bonds. The means of Si–O distances in all the compounds are scattered over the narrow range of 1.613(5) Å to 1.624(5) Å, with the Mg-doped compounds having slightly smaller average Si–O distances. The mean O–O distances in the SiO_4 tetrahedra are $\sim$2.64(2) Å, and like the values of the mean O–Si–O angles, $\sim$109(1)° (Table 5), are independent of the dopant cation.

Table 4. Selected interatomic distances (Å) in β-$Ca_{2-x}M_xSiO_4$, M = Mg and Sr.

	$\beta-Ca_2SiO_4$			
Atoms	x/a	y/b	z/c	B (Å^2)
$M(1)$	0.2717(4)	0.3421(3)	0.5692(2)	0.39(6)
$M(2)$	0.2775(4)	0.9977(3)	0.2982(2)	0.29(6)
Si	0.2327(5)	0.7815(3)	0.5821(3)	0.21(7)
O(1)	0.2870(9)	0.0118(8)	0.5568(5)	0.5(1)
O(2)	0.021(1)	0.7488(8)	0.6912(6)	0.8(1)
O(3)	0.483(1)	0.6688(8)	0.6365(6)	0.9(1)
O(4)	0.1556(9)	0.6737(8)	0.4300(6)	0.6(1)

	$\beta-Ca_{1.99}Sr_{0.01}SiO_4$				$\beta-Ca_{1.975}Sr_{0.025}SiO_4$			
Atoms	x/a	y/b	z/c	B (Å^2)	x/a	y/b	z/c	B (Å^2)
$M(1)$	0.2723(3)	0.3418(3)	0.5694(2)	0.23(6)	0.2709(4)	0.3419(3)	0.5694(2)	0.20(7)
$M(2)$	0.2775(3)	0.9974(3)	0.2980(2)	0.27(6)	0.2769(4)	0.9473(3)	0.2985(2)	0.32(7)
Si	0.2330(5)	0.7813(3)	0.5822(3)	0.15(7)	0.2333(6)	0.7810(4)	0.5821(4)	0.18(8)
O(1)	0.2879(9)	0.0105(8)	0.5574(5)	0.4(1)	0.287(1)	0.0115(9)	0.5563(6)	0.6(1)
O(2)	0.020(1)	0.7496(8)	0.6907(6)	0.9(1)	0.021(1)	0.7488(9)	0.6890(7)	0.8(2)
O(3)	0.4829(1)	0.6695(8)	0.6368(6)	0.6(1)	0.481(1)	0.6698(9)	0.6368(7)	1.1(2)
O(4)	0.1555(9)	0.6730(8)	0.4290(6)	0.7(1)	0.156(1)	0.6733(9)	0.4289(6)	0.5(5)

	$\beta-Ca_{2-x}Mg_xSiO_4$, x =		$\beta-Ca_{2-x}Sr_xSiO_4$, x =		
	0.025	0.01	0	0.01	0.025
M(1)–O(1)	2.241(3)	2.236(3)	2.236(6)	2.244(5)	2.239(6)
M(1)–O(2)	2.508(3)	2.511(3)	2.504(6)	2.508(6)	2.526(7)
M(1)–O(3)	2.435(3)	2.436(3)	2.430(7)	2.432(6)	2.444(7)
M(1)–O(4)	2.359(3)	2.359(3)	2.355(6)	2.359(5)	2.359(6)
M(1)–O(2)′	2.867(3)	2.866(3)	2.870(6)	2.870(6)	2.857(7)
M(1)–O(3)′	2.548(3)	2.553(3)	2.548(6)	2.555(6)	2.546(7)
M(1)–O(4)′	2.649(3)	2.645(3)	2.640(5)	2.646(5)	2.643(6)
Mean$M(1)$–O	2.52(8)	2.52(8)	2.51(8)	2.52(8)	2.52(8)
M(2)–O(1)	2.413(3)	2.414(3)	2.405(5)	2.413(5)	2.400(6)
M(2)–O(2)	2.379(3)	2.375(3)	2.381(6)	2.377(6)	2.384(7)
M(2)–O(3)	2.410(3)	2.411(3)	2.405(6)	2.405(6)	2.414(6)
M(2)–O(4)	2.466(3)	2.466(3)	2.485(6)	2.477(6)	2.482(6)
M(2)–O(1)″	2.660(3)	2.663(3)	2.659(5)	2.654(5)	2.666(6)
M(2)–O(2)″	2.387(3)	2.392(3)	2.402(6)	2.404(6)	2.414(7)
M(2)–O(3)″	2.652(3)	2.648(3)	2.657(6)	2.656(6)	2.663(7)
M(2)–O(4)″	2.616(2)	2.620(3)	2.621(6)	2.621(6)	2.615(6)
Mean$M(2)$–O	2.50(4)	2.50(4)	2.50(4)	2.50(4)	2.50(4)
Si–O(1)	1.596(3)	1.599(3)	1.604(6)	1.589(6)	1.608(6)
Si–O(2)	1.635(4)	1.633(4)	1.619(7)	1.620(7)	1.609(7)
Si–O(3)	1.622(3)	1.627(3)	1.618(6)	1.617(6)	1.607(6)
Si–O(4)	1.633(3)	1.636(3)	1.619(6)	1.631(6)	1.629(6)
Mean Si–O	1.622(9)	1.624(5)	1.614(9)	1.614(5)	1.613(5)
O(1)–O(2)	2.678(4)	2.688(6)	2.674(7)	2.666(7)	2.676(8)
O(1)–O(3)	2.632(4)	2.637(4)	2.636(7)	2.624(7)	2.630(8)
O(1)–O(4)	2.652(4)	2.612(4)	2.644(8)	2.651(8)	2.656(8)
O(2)–O(3)	2.695(4)	2.697(4)	2.685(8)	2.691(7)	2.659(9)
O(2)–O(4)	2.674(4)	2.672(4)	2.645(7)	2.654(7)	2.648(8)
O(3)–O(4)	2.544(4)	2.548(4)	2.529(7)	2.541(7)	2.526(8)
Mean O–O	2.65(2)	2.64(2)	2.64(2)	2.64(2)	2.63(2)

Table 5. Selected bond angles (°) in β-$Ca_{2-x}M_xSiO_4$, M = Mg and Sr.

	$\beta-Ca_{2-x}Mg_xSiO_4$, x =		$\beta-Ca_{2-x}Sr_xSiO_4$, x =		
	0.025	0.01	0	0.01	0.025
O(1)–Si–O(2)	111.6(2)	112.0(2)	112.1(3)	111.9(3)	112.2(3)
O(1)–Si–O(3)	109.9(2)	109.8(2)	109.8(3)	109.4(3)	110.1(3)
O(1)–Si–O(4)	110.7(2)	110.5(2)	110.3(3)	110.4(3)	110.1(3)
O(2)–Si–O(3)	111.9(2)	111.7(4)	112.1(3)	112.5(3)	111.7(4)
O(2)–Si–O(4)	109.7(2)	109.7(2)	109.6(3)	109.5(3)	109.5(3)
O(3)–Si–O(4)	102.9(2)	102.8(2)	102.8(3)	102.9(3)	103.0(4)
Mean O–Si–O	109(1)	109(1)	109(1)	109(1)	109(1)

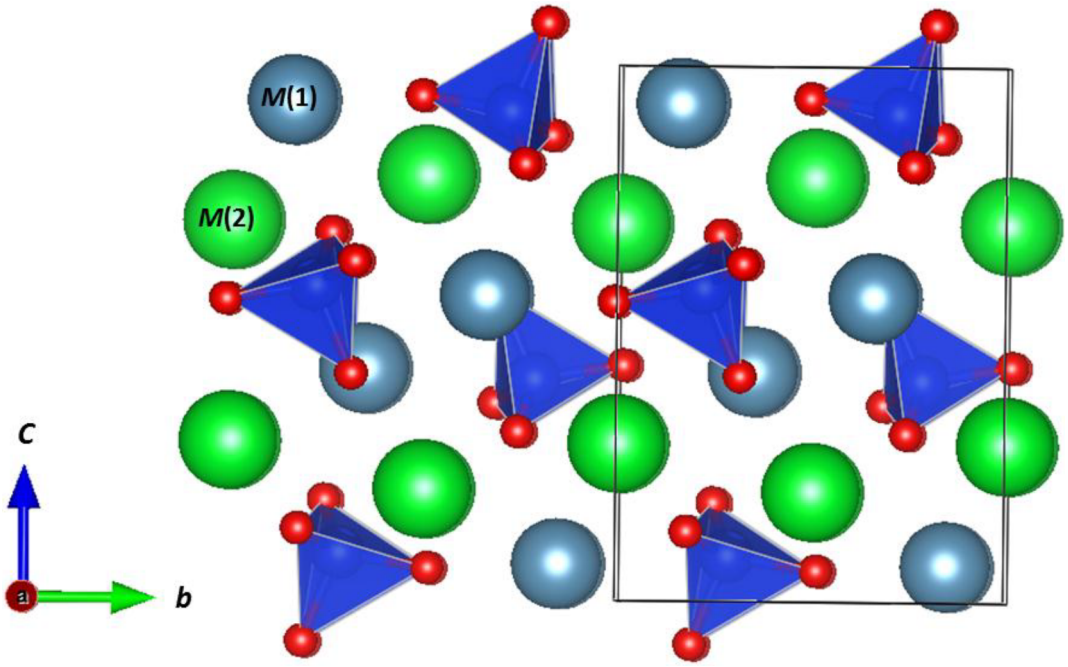

Figure 5. Representation of the β-$Ca_{2-x}M_xSiO_4$ structure. The $M(1)$ and $M(2)$ sites are indicated. The oxygen atoms are at the corners of the tetrahedral SiO_4 groups.

In general the geometry of the SiO_4 tetrahedra in all the compositions studied are very similar and our results are in excellent agreement with those of Jost et al.[17]

In contrast to the consistency of the Si–O bonds, the bond lengths within the two Ca polyhedra vary over a wide range of values, although the averages are remarkably constant (Table 4). These features can be related to local bonding effects and may be quantified by valence bond sums as listed in Table 6. The bond valence calculation shows that the Ca(1) sites are underbonded and each oxygen atom contributes a relatively small bond valence to the Ca(1) sites; rather, for the O atoms, the strongest interaction is with the Si atoms. Conversely, the valence bond sums for the Ca(2) site are unexceptional.

The structural refinements demonstrate that the smaller Mg^{2+} cations have a preference for the $M(1)$ sites in the β-Ca_2SiO_4 structure (Table 2). This is somewhat surprising since the mean $M(1)$–O distance is longer than the mean $M(2)$–O distance and the $M(1)$ site is underbonded. It might, therefore, have been expected that the smaller Mg cations would preferentially occupy the $M(1)$ sites. Conversely, the refinements

Table 6. Valence bond sums of β-$Ca_{2-x}M_xSiO_4$.

	$\beta-$ $Ca_{1.975}Mg_{0.025}SiO_4$	$\beta-Ca_{1.99}Mg_{0.01}SiO_4$	$\beta-Ca_2SiO_4$	$\beta-$ $Ca_{1.99}Sr_{0.01}SiO_4$	$\beta-$ $Ca_{1.975}Sr_{0.025}SiO_4$
Ca(1)	1.79	1.80	1.81	1.79	1.78
	1.74*	**1.75***			
$M(1)$	0.85	0.86	-	-	-
Ca(2)	2.00	1.99	1.97	1.98	1.96
				2.02*	**2.03***
$M(2)$	-	-	-	2.97	2.94
Si	3.74	3.71	3.80	3.81	3.82

*Bold values indicate average values obtained using the refined site occupancies.

suggest that the larger Sr^{2+} cations preferentially occupy the smaller $M(2)$ site. While the average valence bond sum for the $M(2)$ site is not unusual, it is evident from Table 2 that at a local level the Sr ions in this site will be considerably overbonded. Likewise, the Mg ions in the $M(1)$ site are considerably underbonded. Clearly, the valence bond sums provide a rationale for the observed low levels of Mg and Sr substitution, although they do not help to explain the observed site preferences.

2.4. Conclusions

Single-phase samples of $Ca_{2-x}M_xSiO_4, M$ = Mg and Sr, with the β-Ca_2SiO_4 structure have been successfully prepared from $CaCO_3$, SiO_2, and MCO_3 by prolonged heating at 950 °C. The powder diffraction patterns show that these silicates are all isostructural and the structures have been refined in the monoclinic space group, $P2_1/n$. As expected based on size arguments, the cell parameters increase as the amount of Sr increases and likewise decrease as the amount of Mg increases due the size effects of the dopant cation. In all cases the SiO_4 tetrahedra are essentially regular. For both the Sr- and Mg-doped series, the solubility limit of the dopant cation is relatively low, i.e. $\sim$0.025. This can be explained by examination of the valence bond sums.

3. Experimental

3.1. Sample preparation

All samples were prepared by conventional solid-state reaction methods. β-Dicalcium silicate (β-Ca_2SiO_4) was prepared by heating stoichiometric amounts of SiO_2 (Riedel-de Haën) and $CaCO_3$ (Merck, 99.5%) at 950 °C for 4 h. The sample was then air-quenched to room temperature to avoid the formation of γ-Ca_2SiO_4. Magnesium-doped β-dicalcium silicate (β-$Ca_{2-x}Mg_xSiO_4$, x = 0.01, 0.025, 0.04, 0.05, 0.1, and 0.25) and strontium-doped β-dicalcium silicate (β-$Ca_{2-x}Sr_xSiO_4$, x = 0.01, 0.025, 0.05, and 0.1) were prepared by the solid-state reaction of stoichiometric amounts of $MgCO_3$ (BDH) or $SrCO_3$ (Merck, 98.5%), $CaCO_3$ (Merck, 99.5%), and SiO_2 (Riedel-de Haën) at 950 °C for 4 h followed by air-quenching.

3.2. Structure measurements and analysis

The formation of the targeted phases was monitored by powder X-ray diffraction using a Siemens D-5000 Diffractometer and the wavelength of the X-ray CuKα = 1.54178 Å. Synchrotron X-ray diffraction data were collected on a Debye Scherrer diffractometer at the Australian National Beamline Facility and Beamline 20B at the Photon Factory, Tsukuba, Japan.[32,33] The sample was housed in a capillary of 0.3 mm in diameter that was rotated during the measurements. Wavelengths (λ) used in synchrotron X-ray diffraction data collections

of β-Ca_2SiO_4, β-$Ca_{2-x}Mg_xSiO_4$ (x = 0.01 and 0.025), and β-$Ca_{2-x}Sr_xSiO_4$ (x = 0.01 and 0.025) were 0.99418 Å, 0.99868 Å, and 0.99702 Å, respectively. EDA was performed with an EDAX PV9900 system on a Phillips 505 scanning microscope operating at 20 keV. The samples were mounted using carbon tape and coated with either Pt (for collecting images) or C (for EDA) to reduce charging effects.

All structures were refined by the Rietveld method,[34] using the program LHPM.[35] The structures of the doped samples β-$Ca_{2-x}M_xSiO_4$, M = Mg or Sr, were refined using synchrotron powder X-ray diffraction data. In all cases it was possible to obtain satisfactory fits using a single-phase model, although a small amount of poorly crystalline SiO_2 was present in some samples. The structural parameters reported by Jost et al.[17] for monoclinic space group $P2_1/n$, β-Ca_2SiO_4, were used as a starting model. Up to 51 parameters, including positional, profile, and background parameters, were used in the refinements.

Acknowledgments

This work was partially supported by the Australian Research Council. The synchrotron measurements at the Australian National Beamline Facility were supported by the Australian Synchrotron Research Program, which is funded by the Commonwealth of Australia under the Major National Research Facilities program. We thank Drs James Hester and Garry Foran for their assistance with these measurements.

References

1. Wen, J.; Yeung, Y. Y.; Ning, L. X.; Duan, C. K.; Huang, Y. C.; Zhang, J.; Yin, M. *J. Lumin.* **2016**, *178*, 121-127.
2. Popescu, C. D.; Muntean, M.; Sharp, J. H. *Cem. Concr. Compos.* **2003**, *25*, 689-693.
3. Chen, Y. L.; Shih, P. H.; Chiang, L. C.; Chang, Y. K.; Lu, H. C.; Chang, J. E. *J. Hazard. Mater.* **2009**, *170*, 443-448.
4. Barbier, J.; Hyde, B. G. *Acta Crystallogr. B* **1985**, *41*, 383-390.
5. Eysel, W.; Hahn, T. *Z. Kristallogr. Kristallgeom. Kristallphys. Kristallchem.* **1970**, *131*, 322.
6. Ishida, H.; Mabuchi, K.; Sasaki, K.; Mitsuda, T. *J. Am. Ceram. Soc.* **1992**, *75*, 2427-2432.
7. Saalfeld, H. *Am. Mineral.* **1975**, *60*, 824-827.
8. Yamazaki, S.; Toraya, H. *Powder Diffr.* **2001**, *16*, 110-114.
9. Nettleship, I.; Shull, J. L.; Kriven, W. M. *J. Eur. Ceram. Soc.* **1993**, *11*, 291-298.
10. Roy, D. M.; Oyefesobi, S. O. *J. Am. Ceram. Soc.* **1977**, *60*, 178-180.
11. Xiong, Z. H.; Liu, X.; Shieh, S. R.; Wang, S. C.; Chang, L. L.; Tang, J. J.; Hong, X. G.; Zhang, Z. G.; Wang, H. J. *Am. Mineral.* **2016**, *101*, 277-288.
12. Kralj, D.; Matkovic, B.; Trojko, R.; Young, J. F.; Chan, C. J. *J. Am. Ceram. Soc.* **1986**, *69*, C170-C172.
13. Lai, G. C.; Nojiri, T.; Nakano, K. *Cem. Concr. Res.* **1992**, *22*, 743-754.
14. Cuesta, A.; Aranda, M. A. G.; Sanz, J.; de la Torre, A. G.; Losilla, E. R. *Dalton Trans.* **2014**, *43*, 2176-2182.
15. Tilley, C. E. *Min. Mag.* **1929**, *22*, 77-86.
16. Cruickshank, D. W. *Acta Crystallogr.* **1964**, *17*, 685-686.
17. Jost, K. H.; Ziemer, B.; Seydel, R. *Acta Crystallogr. B* **1977**, *33*, 1696-1700.
18. Midgley, C. M. *Acta Crystallogr.* **1952**, *5*, 307-312.
19. Mumme, W.; Cranswick, L.; Chakoumakos, B. *Neues Jahrb. Mineral. Abh.* **1996**, *170*, 171-188.
20. Mumme, W. G.; Hill, R. J.; Bushnell-Wye, G.; Segnit, E. R. *Neues Jahrb. Mineral. Abh.* **1995**, *169*, 35-68.

21. Yamnova, N. A.; Zubkova, N. V.; Eremin, N. N.; Zadov, A. E.; Gazeev, V. M. *Crystallogr. Rep.* **2011**, *56*, 210.
22. Berliner, R.; Ball, C.; West, P. B. *Cem. Concr. Res.* **1997**, *27*, 551-575.
23. Horiuchi, H.; Sawamoto, H. *Am. Mineral.* **1981**, *66*, 568-575.
24. Irifune, T.; Nishiyama, N.; Kuroda, K.; Inoue, T.; Isshiki, M.; Utsumi, W.; Funakoshi, K.; Urakawa, S.; Uchida, T.; Katsura, T. et al. *Science* **1998**, *279*, 1698-1700.
25. Carlson, E. T. *J. Res. Nat. Bur. Stand.* **1955**, *54*, 329.
26. Bickle, M. J. *Nature* **1994**, *367*, 699-704.
27. Catti, M.; Gazzoni, G. *Acta Crystallogr. B* **1983**, *39*, 679-684.
28. Catti, M.; Gazzoni, G.; Ivaldi, G. *Acta Crystallogr. C* **1983**, *39*, 29-34.
29. Catti, M.; Gazzoni, G.; Ivaldi, G. *Acta Crystallogr. B* **1984**, *40*, 537-544.
30. Sakurada, R.; Kawazoe, Y.; Singh, A. K. *ACI Mater. J.* **2015**, *112*, 85.
31. Lu, Z. Y.; Tan, K. F. *Cem. Concr. Res.* **1997**, *27*, 989-993.
32. Garrett, R. F.; Cookson, D. J.; Foran, G. J.; Sabine, T. M.; Kennedy, B. J.; Wilkins, S. W. *Rev. Sci. Instrum.* **1995**, *66*, 1351-1353.
33. Sabine, T. M.; Kennedy, B. J.; Garrett, R. F.; Foran, G. J.; Cookson, D. J. *J. Appl. Crystallogr.* **1995**, *28*, 513-517.
34. Rietveld, H. M. *J. Appl. Crystallogr.* **1969**, *2*, 65-71.
35. Hunter, B. A.; Howard, C. J. *A Computer Program for Rietveld Analysis of X-Ray and Neutron Powder Diffraction Patterns*; Australian Atomic Energy Commission: Lucas Heights, Australia, 1998.